ACS APPLIED MATERIALS & INTERFACES

Research Article

www.acsami.org

Impact of 3D Hierarchical Nanostructures on the Antibacterial Efficacy of a Bacteria-Triggered Self-Defensive Antibiotic Coating

Ferdi Hizal,[†,‡] Iryna Zhuk,[§] Svetlana Sukhishvili,[§,#] Henk J. Busscher,[‡] Henny C. van der Mei,[‡] and Chang-Hwan Choi*[,†]

[†]Department of Mechanical Engineering and [§]Department of Chemistry, Chemical Biology and Biomedical Engineering, Stevens Institute of Technology, Castle Point on Hudson, Hoboken, New Jersey 07030, United States

[‡]Department of Biomedical Engineering (FB40), University of Groningen and University Medical Center Groningen, Antonius Deusinglaan 1, 9713 AV Groningen, The Netherlands

Supporting Information

ABSTRACT: Titanium is often applied in implant surgery, but frequently implicated in infections associated with bacterial adhesion and growth on the implant surface. Here, we show that hierarchical nanostructuring of titanium and the subsequent coating of resulting topographical features with a self-defensive, antibacterial layer-by-layer (LbL) film enables a synergistic action of hierarchical nanotopography and localized, bacteria-triggered antibiotic release to dramatically enhance the antibacterial efficiency of surfaces. Although sole nanostructuring of titanium substrates did not significantly affect adhesion and growth of *Staphylococcus aureus*, the coating of 3D-nanopillared substrates with an ultrathin tannic acid/gentamicin (TA/G) LbL film resulted in a 10-fold reduction of the number of surface-attached bacteria. This effect is attributed to the enlarged surface area of the nanostructured coating available for localized bacteria-triggered release of antibiotics, as well as to the lower bacterial adhesion forces resulting in subsided activation of bacterial antibiotic-defense mechanisms when bacteria land on nanopillar tips. The result shows that a combination of 3D nanostructuring with a bacteria-triggered antibiotic-releasing coating presents a unique way to dramatically enhance antibacterial efficacy of biomaterial implants.

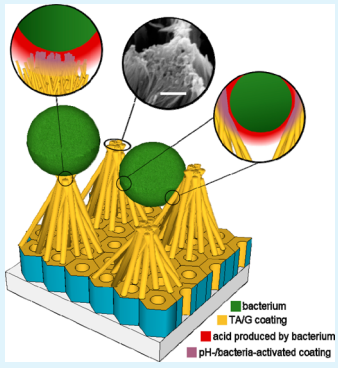

KEYWORDS: *biomaterial, titanium, nanostructure, antibacterial coating, bacterial adhesion*

INTRODUCTION

Titanium (Ti) is a frequently employed material in modern medicine such as in orthopedic trauma surgery and for use in total hip- and knee-arthroplasties or dental implants. Despite the fact that titanium is well-tolerated by the body, titanium implants are prone to bacterial adhesion and growth ("biofilm formation").[1,2] Once a biomaterial implant has become colonized by bacteria, the biofilm mode of growth protects the inhabiting organisms against the host immune system and antibiotic attack.[3] For many clinically used antibiotics, the antibiotic concentration required to kill bacteria in a biofilm mode of growth is orders of magnitude higher than tolerated by the human body.[4] Hence local antibiotic delivery systems are employed more and more as they yield high antibiotic concentrations in the immediate vicinity of an implant threatened by infection while avoiding harmfully high concentrations elsewhere in the body. Gentamicin is a commonly used antibiotic in local delivery systems, typically applied in porous beads or biodegradable coatings.[5] They release their gentamicin content ad libitum, making a high burst release followed by a low level tail-release that can continue for years.[6] As a result, many bacterial strains and species have become resistant to gentamicin.[7] To overcome such issues, several types of layer-by-layer (LbL) polymer coatings[8] that incorporate antibacterial compounds and continuously release them in a highly localized manner have been explored.[9−14] One of the ways has been using pH-responsive drug delivery systems such as pH-responsive coatings.[15−17] A significant recent development includes a new family of LbL coatings, which do not elute antibiotics under normal, infection-free conditions, but supply antibiotics locally only when activated by bacteria-induced pH lowering.[18]

A different approach explored for the prevention of bacterial adhesion and biofilm formation that has yet to find its way to clinical use is to engineer surface topography and wettability (Table 1). Especially, using antifouling pillar-patterned poly(ethylene glycol) hydrogels, Wang et al. show that adhesion of staphylococci was significantly reduced for the surface patterns with interpillar spacing below 1.5 μm.[19] Above the critical pattern periodicity of 1.5 μm, the bacteria did not show a significant change in their adhesion behavior, which suggests that the critical length scale for effective prevention of bacterial adhesion on these bacteria-repulsive surfaces falls to the scale smaller than the size of a bacterium.[19] Prior works on

Received: July 2, 2015
Accepted: August 25, 2015
Published: August 25, 2015

DOI: 10.1021/acsami.5b05947
ACS Appl. Mater. Interfaces 2015, 7, 20304−20313

Table 1. Prior Works on the Effect of Micro/Nanostructured Surfaces on Bacterial Adhesion[a]

	surface pattern								
ref	material	regularity	shape	scale	dimensions (λ, t or d, h)	surface coating or treatments	surface wettability	bacteria type	main results
Bos et al. (2000)[20]	glass	regular	line	micro	λ = 30 μm, t = 10 μm	dimethyldichlorosilane (DDS)	hydrophobic	*S. sobrinus*	same number of adherence on both hydrophilic and hydrophobic surface; however, air bubble detached more bacteria from hydrophobic surfaces
Popat et al. (2007)[21]	TiO_2	regular	tube	nano	d = 80 nm, h = 400 nm	gentamicin loading into nanotubes	hydrophilic	*S. epidermis*	decreased adhesion on nanotubes filled with gentamicin, compared to bare Ti and nanotubes with no gentamicin filled
Puckett et al. (2010)[22]	TiO_2	random & regular	random: roughness, regular: tube	nano	roughness: R_a = 50 nm, tube: d = 80 and 200 nm	NA	hydrophilic	*S. aureus, S. epidermidis, P. aeruginosa*	decreased bacteria colonies on nanorough and conventional Ti, compared to nanotubular and nanotextured Ti
Wang et al. (2011)[19]	PEG hydrogel	regular	pillar	micro & nano	λ = 0.5−3.0 μm, t = 400 nm, h = 120 nm	NA	hydrophilic	*S. aureus*	Reduced bacteria adhesion below λ = 1.5 μm.
Ercan et al. (2011)[23]	TiO_2	regular	tube	nano	d = 20−80 nm	heat treatment	hydrophilic	*S. epidermidis, S. aureus*	reduced bacteria adhesion on heat-treated 80 nm nanotubular, compared to untreated one
Wu et al. (2011)[24]	Ti alloy	random	roughness	micro & nano	R_a = 33, 11, 0.83 μm and 6 nm	NA	hydrophilic	*S. epidermidis*	reduced bacteria adhesion at R_a= 33 μm and R_a = 6 nm
Tang et al. (2011)[25]	TiO_2	regular	tube	nano	d = 80 nm, h = 400 nm	PTES	superhydrophobic	*S. aureus*	reduced adhesion on flat hydrophobic Ti and more on superhydrophobic nanotubular surfaces compared to hydrophilic nanotubular surface
Ivanova et al. (2013)[26]	SiO_2	regular	pillar	nano	λ = 200 nm, t = ∼50 nm, h = 500 nm	NA	hydrophilic	*P. aeruginosa, S. aureus, B. subtilis*	nanopillars effectively killed bacteria by rupturing cell membrane (killing rate up to ∼450 000 cells/cm^2 per minute)
Hizal et al. (2014)[27]	Al_2O_3	regular	pore & pillar	nano	pore: d = 30 nm, h = 1.5 μm; pillar: λ = 1 μm, t = 200 nm, h = 1 μm	Teflon	superhydrophobic	*S. aureus, E. coli*	little adherence on superhydrophobic surfaces, compared to hydrophilic surfaces

[a] λ, structural pitch; t, tip size (for line or pillar); d, diameter (for tube or pore); h, height or depth; PEG, poly(ethylene glycol); PTES; 1H, 1H, 2H, 2H-perfluorooctyl-triethoxysilane

ACS Appl. Mater. Interfaces 2015, 7, 20304−20313 DOI: 10.1021/acsami.5b05947

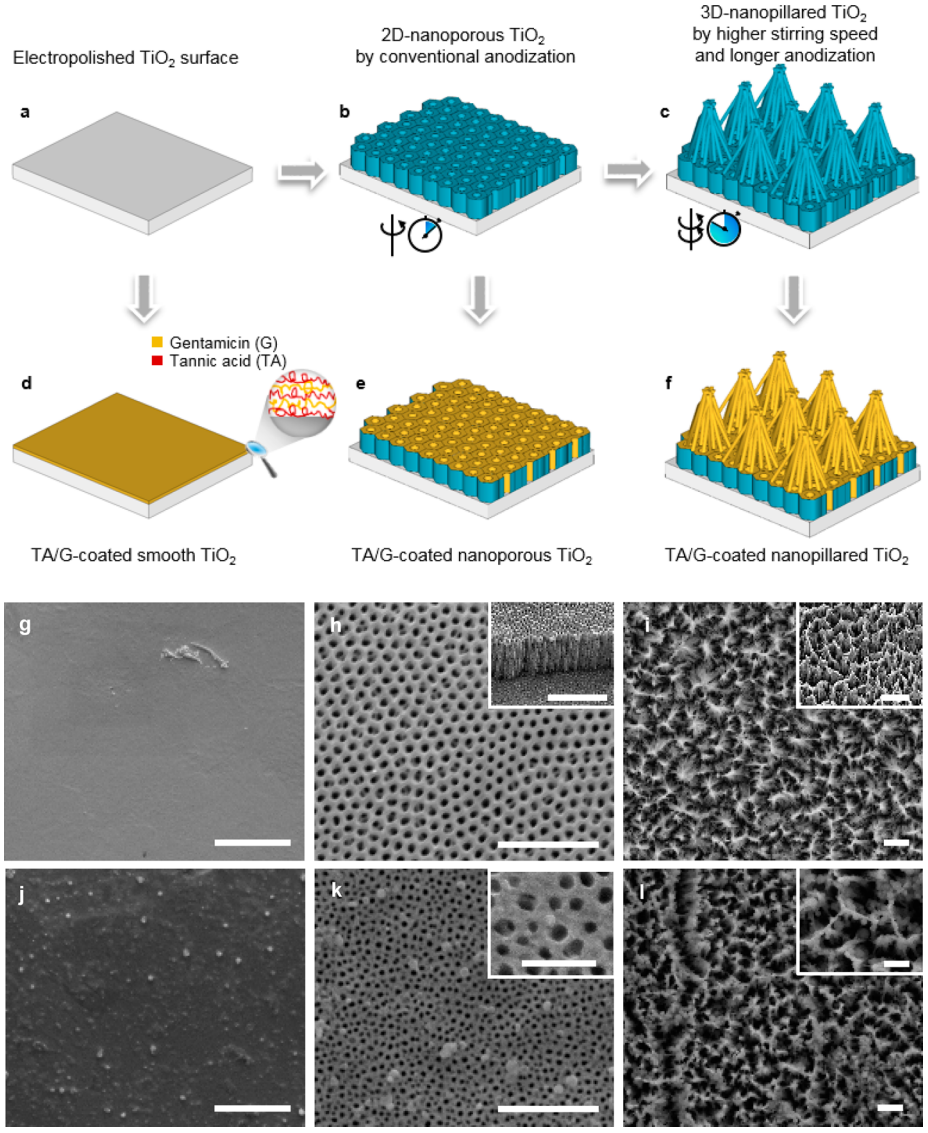

Figure 1. Fabrication of nanostructured TiO_2 surfaces with gentamicin-releasing coating. (a) Electropolished TiO_2 with a smoothened surface is anodized with a conventional anodizing method to produce (b) a 2D-nanoporous surface. Further anodization at a higher stirring speed results in (c) a 3D-nanopillared surface. (d–f) The resulting surfaces are then coated using the LbL deposition of tannic acid (TA) and gentamicin (G). Scanning electron micrographs (top views) show (g, j) smooth, (h, k) 2D-nanoporous, and (i, l) 3D-nanopillared TiO_2 surfaces in absence (top row) or presence (bottom row) of the gentamicin-releasing TA/G LbL coating. The scale bar in each micrograph represents 1 μm. Insets in h and i show the titled views, where the scale bars represent 2 μm. Insets in k and l show the top views of high-magnification details, where the scale bars represent 500 nm.

nanostructured titanium oxide (TiO_2) surfaces also showed some reduction of bacterial adhesion, growth, and viability, which were ascribed to Ti crystallinity, its modified surface chemistry, and photocatalytic activity.[28,23] Direct loading of unbound gentamicin within the titanium oxide nanotubes further enhanced the substrate antibacterial properties.[21] However, it should be noted that titanium oxide nanostructures of different morphology and size showed the opposite effect, increasing bacteria colonization.[22] Effective bacterial killing was also reported for a nanopillared black silicon substrate as a result of the mechanical rupture of the bacterial cell membrane by the sharp and hydrophilic nanopillars.[26] Other works have also shown the combined effects of the nanostructure and surface wettability, demonstrating suppressed adhesion of bacteria due to substrate-entrapped air and a reduced bacteria-solid contact area.[27,25] Although several studies demonstrated a possibility of controlling bacterial adhesion and growth or even triggering bacterial death via nanostructures, the role of the surface nanostructure features on bacterial attachment has not yet been systematically explored for the case when surface nanostructures work side-by-side with antibiotic-containing coatings, especially for self-defensive coating that release antibiotics locally only when it is triggered by bacteria-surface interaction.

This work explores the relative contributions and synergistic effects on bacterial adhesion and growth of surface topography and a "smart", self-defensive ultrathin coating, which releases antibiotic on demand in response to bacterial presence. A 3D nanostructure landscape can provide unique interactions of planktonic bacteria with a surface. As bacteria lands on a sharp ends of 3D surface nanostructures such as pillars, a decrease in the effective contact area might result in lowering of the

DOI: 10.1021/acsami.5b05947
ACS Appl. Mater. Interfaces 2015, 7, 20304–20313

bacteria−substrate adhesion force as compared to that on a flat substrate. On the other hand, when the distance between surface features is larger than the bacterial size, deposition of bacteria within the valleys and adhesion through multiple contact points is also expected. For uncoated surfaces, these two routes might have opposite effects on the overall population of surface by bacteria. Specifically, smaller adhesion contact area (interaction with the high-aspect-ratio 3D nanostructure) should suppress bacterial adhesion, whereas surface roughness at microscopic length scales leads to enhanced accumulation of bacteria in surface valleys, depressions and pits.[24] The main goal of this work is to explore whether coatings of the micro/nanostructured substrates with a smart, bacteria-triggered coating that deliver antibiotics to bacterial on demand in a highly localized way can invert these opposing trends and recruit both nanoscopic and microscopic surface features to become efficiently antibacterial. To that end, we modify an electrochemical anodizing process[29] to create 3D nanopillared TiO_2 nanostructures on titanium substrate, and explore bacteria adhesion properties of as-prepared, as well as LbL-coated substrates. The coating of our choice is composed of tannic acid (TA) and gentamicin (G). As recently demonstrated, TA/G films are completely noneluting at pH 7.4, but become antibiotic-delivering when local pH is acidified by acid-producing bacteria, such as *S. epidermidis*, *S. aureus* or *.E. coli*.[18] Here, we concentrate on *S. aureus* as one of the most common for hip- or knee-implant-associated infections. A clinical isolate from pleural fluid, a gentamicin-sensitive strain of ATCC 12600 is selected due to its known culture characteristics, pathogenicity and adhesion properties (producing slime and forming biofilm). Antibacterial efficacy is assessed with fluorescence microscopy by determining the number and viability of *S. aureus* ATCC 12600 adhering to coated and uncoated nanostructured surfaces, respectively, and compared with the results on electropolished smooth TiO_2 surfaces as well as 2D-nanoporous surfaces.

RESULTS AND DISCUSSION

Electrochemical anodizing provides a facile and inexpensive means to create nanostructures over large areas of metallic surfaces. Significantly, this includes surfaces of complex geometries that are ubiquitous in biomedical implants or devices,[30] but not amendable to lithographic approaches.[31] The overall fabrication schemes, yielding smooth, 2D-nanoporous, or 3D-nanopillared TiO_2 surfaces are shown in Figures 1a−c. Electropolished smooth (average surface roughness, R_a = 33 ± 13 nm, measured over 75 μm^2) TiO_2 surfaces (Figure 1a) are employed for the nanostructured TiO_2 surfaces. The topography of surface nanostructures (e.g., from a 2D-nanoporous layer to a 3D-nanopillared array) can be conveniently controlled by the anodizing conditions, i.e., anodization time and stirring speeds (Figures 1b, c). Figures 1g−i show the fabricated nanostructures, resulted from following the different schemes illustrated in Figures 1a−c. A conventional anodizing process resulted in a 2D-nanoporous layer of TiO_2 (Figure 1h), with an average pore diameter of 55 nm, an interpore distance of 70 nm, and a depth of 1 μm. In contrast, a 10-fold increase in the anodization stirring rate and a 15-fold extension of the process duration as compared to conventionally used procedures resulted in distinct 3D-nanopillared surface features. Preparation of 3D-nanopillared TiO_2 substrates involves continuous exposure of forming oxides to a shear-stresses-generated drag force.[32] At increased stirring rates, the drag force creates tension on the mechanically weak points, leading to the preferential chemical dissolution of TiO_2 by F^- etching.[33,34] As a result, the upper parts of 2D-nanoporous TiO_2 structures thin, collapse, and split to form first individual, and then bundled 3D nanopillars.[35] In this study, the conical bundled nanopillars with an average distance of 2 μm, a bundled tip diameter of 10 nm, and a height of 2 μm were created (Figure 1i). On the basis of the geometric dimensions and shapes of the surface topographies, the 2D-nanoporous and 3D-nanopillared topographies were estimated to have about 20-fold and 100-fold larger surface area as compared to that of a smooth surface, respectively. In addition to the increased surface area, the hierarchically nanostructured substrates cover a wide scale of nano- and microdimensions, offering various adhesion opportunities for bacterial adhesion. The apparent contact angles of a sessile water droplet (a few microliters) on the smooth, 2D-nanoporous, and 3D-nanopillared TiO_2 surfaces were ∼40, ∼15, and ∼0°, respectively, indicating the surfaces are highly hydrophilic.

After the three different surface topographies (i.e., smooth, 2D-nanoporous, and 3D-nanopillared) were prepared, nine bilayers of antibiotic-containing TA/G film were applied by LbL deposition (Figures 1d−f). Figures 1j−l show the topography of the smooth and two different nanostructured surfaces after LbL coating with TA/G. In the case of a 2D-nanoporous surface (Figure 1k), the average pore diameter was slightly reduced from 55 to 40 nm due to the TA/G coating on the inner walls of the pores. In the case of a 3D-nanopillared surface (Figure 1l), the tip diameter of the bundled conical nanostructures also increased from 10 to 30 nm after the coating deposition, in good agreement with the thickness of 10−15 nm as determined for 9-bilayer TA/G coating deposited on a flat substrate.[18] The apparent contact angles of a sessile water droplet (a few microliters) on the TA/G-coated smooth, 2D-nanoporous, and 3D-nanopillared TiO_2 surfaces were ∼50, ∼ 35, and ∼0°, respectively, indicating the TA/G-coated surfaces are also highly hydrophilic. In contrast to conventional antibiotic coatings that release their antibiotic content ad libitum, bearing the risk of becoming ineffective when bacteria adhere and the antibiotic is needed, the TA/G coating delivers antibiotics on demand, only where and when needed.[18] This coating has three distinct advantages when applied to the orthopedic implants. Its “dormant” nature at pH 7.4, i.e., in the absence of bacteria, assures that the TA/G coating stores antibiotic until contaminating bacteria adhere and lower the local pH to release a fraction of contained antibiotic. Our recent experiments with TA/G coatings deposited on smooth substrates have demonstrated that the coating is noneluting at pH 7.5, but starts releasing increased amounts of gentamicin when pH is lowered between 7.5 and 5.0.[18] The noneluting nature of the TA/G coating at pH 7.4 is important from two standpoints. First, the highly localized, on demand pulsed release minimizes the chances for the development of antibiotic-resistant bacterial strains. Second, it is important that antibiotic is stored within the noneluting coating for prolonged periods of time. Note that infections associated with titanium implants are initiated not only by bacteria contaminating the wound site, but also by spreading of bacteria from infections elsewhere in the body, which can occur at any time, even long after the surgery.[36] It has been shown that this new LbL coating preserves its antibacterial activity even after 35 days, whereas it is nonreleasing its antibiotics for as long as 4 weeks if the pH was stable at 7.5.[18] Meanwhile, the TA/G

DOI: 10.1021/acsami.5b05947
ACS Appl. Mater. Interfaces 2015, 7, 20304−20313

coating has shown nontoxicity and biocompatibility toward mammalian cells such as preosteoblasts cells.[18]

Before the assessment of the antibacterial efficacy of the coated surfaces, we have assessed the noneluting nature and pH-controlled release of gentamicin from the coatings. The TA/G-coated smooth, 2D-nanoporous, and 3D-nanopillared samples (1 cm × 1 cm) were first immersed in 500 μL of potassium phosphate buffered saline (PBS), with pH adjusted to either 5.0 or 7.5. After the immersion for 10, 30, 60, and 120 min, respectively, a droplet (5 μL) of the PBS solution was taken out and subsequently put on tryptone soya agar inoculated with *S. aureus* ATCC 12600 and left for 48 h in an incubator at 37 °C. The development of an inhibition zone around the droplet was taken as an indication of gentamicin release (Figure 2; see also Figure S1). No inhibition zones were

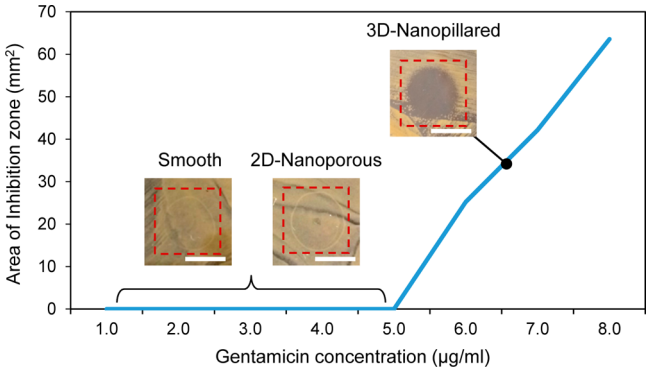

Figure 2. Gentamicin release from TA/G-coated samples using zone of inhibition assays. A calibration curve was prepared relating the area of an inhibition zone developed on an agar plate inoculated with *S. aureus* ATCC 12600 around a 5 μL droplet of PBS (pH 5.0) containing different gentamicin concentrations. Photographs were taken of the inhibition zones developing around the 5 μL PBS droplets after release of gentamicin from TA/G-coated smooth, 2D-nanoporous, and 3D-nanopillared samples. The clear contrast of a circular zone of inhibition shown for a 3D-nanopillared sample is indicative of gentamicin release, and its area (around 35 mm^2) can be related with the amounts of gentamicin released from the coated surfaces per cm^2 using the calibration curve. In the case of the smooth and 2D-nanoporous samples, no clear inhibition zone was found, which suggests the gentamicin concentration is less than 5 μg/mL. Scale bars in photographs indicate 5 mm.

caused by droplets from smooth and 2D-nanoporous samples, regardless of pH and immersion time, suggesting that these aliquots did not release enough gentamicin (less than 5 μg/mL in 0.5 mL; see Figure 2) to develop a visible zone of inhibition. In contrast, a droplet from the immersion of 3D-nanopillared samples at pH 5.0 yielded a clear inhibition zone with an area of 35 mm^2, regardless of immersion time. The latter is consistent with the fast, on-demand release kinetics of the antibiotic from the coating.[18] Importantly, however, no visible inhibition zones developed from a droplet with immersion of 3D-nanopillared samples at pH 7.5. On the basis of a calibration curve that relates the area of an inhibition zone with the amount of gentamicin, release from 3D-nanopillared samples at pH 5.0 corresponds to 3.5 μg/cm^2. The significant release of the gentamicin from 3D-nanopillared surfaces is attributed to the enhanced surface area of the coating on this substrate, which is about 100 times higher than that on a smooth surface, and about 5 times higher than on 2D-nanoporous substrates.

For the assessment of the antibacterial efficacy of the TA/G-coated nanostructured TiO_2 samples, adhesion of *S. aureus* was studied in a parallel plate flow chamber experiments (see Figure S2). The smooth, 2D-nanoporous, and 3D-nanopillared samples were placed in a row in the poly(methyl methacrylate) (PMMA) bottom plate of the chamber and *S. aureus* were allowed to adhere from a flowing suspension for 2 h at a wall shear rate of 6 s^{-1}. Adhering *S. aureus* were then live/dead stained to facilitate enumeration of the numbers of live and dead bacteria adhering on each sample (Figure 3a). For comparison, uncoated and only TA-monolayer coated samples were also included in the enumeration, as well as the PMMA surfaces surrounding the samples. Quantitative data derived from the fluorescent images are shown in Figure 3b. Noticeably, the numbers of live and dead *S. aureus* adhering on the PMMA substrate in the vicinity of coated or uncoated samples are not statistically different. This indicates that gentamicin release and associated staphylococcal killing is highly local, even under convective diffusion conditions in the parallel plate flow chamber experiments. The behaviors of *S. aureus* on gentamicin-free uncoated and TA-coated samples are similar to those on the surrounding PMMA surface. Interestingly, equal total number, as well as live and dead bacteria adhere to uncoated surfaces, regardless of the surface topography. This agrees very well with previous work[19] as *S. aureus* did not change the adherence characteristic above the critical interpillar spacing size of 1.5 μm. In contrast, on TA/G-coated surfaces, adhesion and viability of *S. aureus* are significantly reduced, compared to both uncoated and TA-coated surfaces. The antibacterial effect of the TA/G-coating is more pronounced on the nanostructured surfaces than on the smooth surface. In particular, it is the most dramatic on 3D-nanopillared surfaces, showing about 10-fold reduction in the number of *S. aureus* adhesion in comparison with that on the smooth surface.

Scanning electron micrographs (Figure 4) show the appearance of *S. aureus* adhering on the nanostructured surfaces. In the case of uncoated surfaces (Figures 4a–c), no differences were observed in the appearance of *S. aureus* on the smooth and 2D-nanoporous surfaces (Figures 4a, b, respectively), whereas on 3D-nanopillared surfaces (Figure 4c) staphylococci were found either in crevices or on tips of the bundled nanopillar structures, having multiple contact points. The multiscale features of the hierarchical 3D-nanopillared substrate probably have the opposing trends on the bacterial adhesion, with bacterial adhesion weakened by the nanostructures (nanopillar tops), and bacterial deposition encouraged by the microscale valleys, resulting in the overall inefficiency of the nanostructure itself to control bacterial adhesion. Coating of the substrates with TA/G films reveals dramatic differences in the action of differently nanostructured substrates to adhering bacteria (Figure 3 and Figures 4d–f). In addition to a 10-fold reduction of the total number of bacteria adhered to a 3D-nanopillared surface, there are significant differences in the mode of interaction of different coating-activated nanostructures with bacteria. Staphylococci adhering on TA/G-coated smooth and 2D-nanoporous surfaces (Figures 4d, e, respectively) all have similar undistorted shape, also observed with uncoated surfaces (Figures 4a, b), and the surrounding substrate area appears clean, with negligible amounts of secreted extracellular polymeric substances (EPS). In contrast, in the case of the TA/G-coated 3D-nanopillared surfaces (Figure 4f), much larger patches of EPS were observed around

DOI: 10.1021/acsami.5b05947
ACS Appl. Mater. Interfaces 2015, 7, 20304–20313

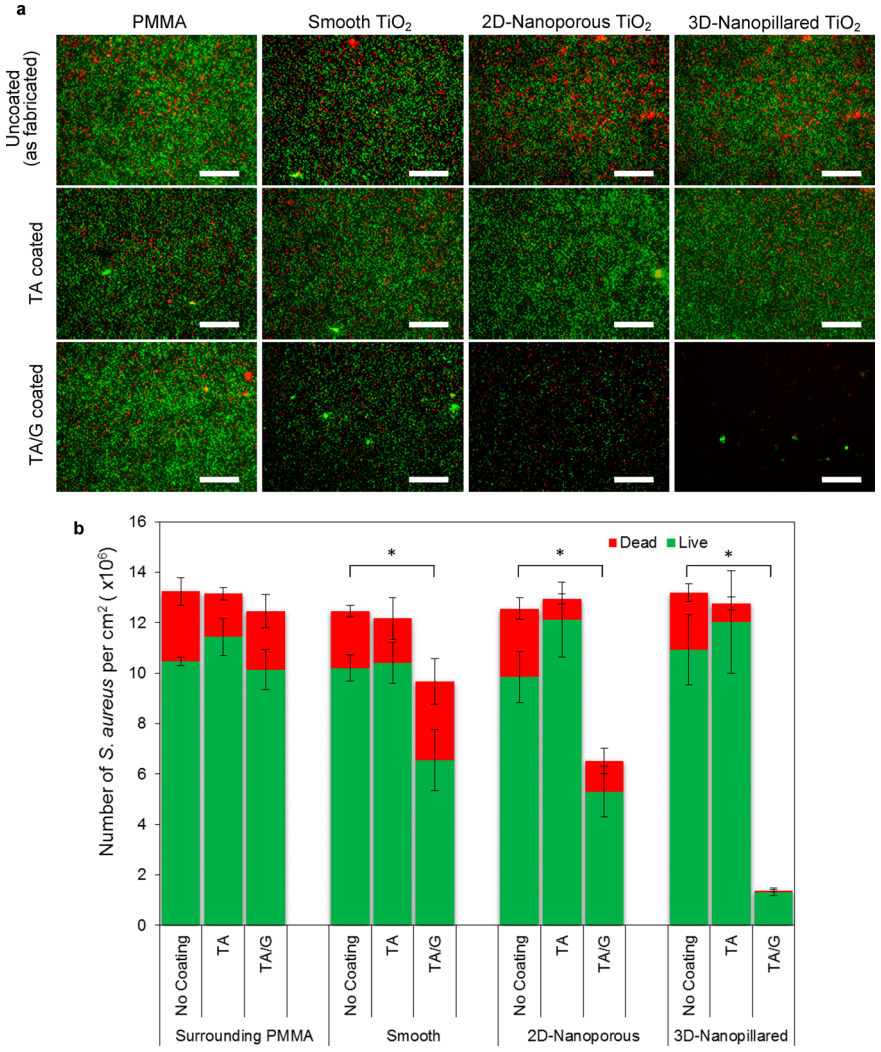

Figure 3. Bacterial adhesion and viability on TiO_2 surfaces. (a) Fluorescent microscope images of live and dead *S. aureus* ATCC 12600 adhering to PMMA, smooth, 2D-nanoporous, and 3D-nanopillared TiO_2 surfaces. Live bacteria appear green-fluorescent, whereas dead bacteria do red. Each image is representative of the images taken out of five different locations on 1 × 1 cm samples. Scale bars = 100 μm. (b) Quantitative data derived from the fluorescent images. Error bars indicate the standard deviations over triplicate experiments, each involving separately prepared surfaces and bacterial cultures. Asterisks indicate statistical significance ($p < 0.005$) between indicated groups. Images and data for PMMA pertain to the live and dead *S. aureus* measured for the bottom PMMA plate of the flow chamber walls (Figure S2), more specifically the areas that surround the uncoated and coated samples. Images and data for TA refer to the live and dead *S. aureus* measured on the gentamicin-free samples coated with only a monolayer of TA.

adhered *S. aureus*, indicating a much stronger bacterial reaction to the antibiotics released.

Deduced from the results, Figure 4g illustrates the mechanism of the enhancement of antibacterial efficacy of the self-defensive bacteria-triggered gentamicin-releasing coating, as substantiated by the hierarchical 3D-nanopillared surface topography. First, because of its unique high-aspect-ratio 3D topography, the 3D-nanopillared TiO_2 surface provides an overall larger surface area for the TA/G-coating (approximately by a factor of 100) than a smooth surface, enabling the deposition of a larger amount of gentamicin per macroscopic surface area unit. Furthermore, as revealed in Figure 4c, *S. aureus* adhering on the 3D-nanopillared surfaces have multiple contact points with nanopillared substrates, residing either in crevices or on bundled tips. The hierarchical 3D-nanopillared surface (Figure 4g) enhances the antibacterial efficacy dramatically through producing higher concentrations of gentamicin released at the local region of the multiple contacts. Yet, the overall amount of gentamicin released from the TA/G coating is dramatically lower (e.g., 3.5 $\mu g/cm^2$ or 3.5×10^{-11} $mg/\mu m^2$, see Figure 2), compared to the amount of gentamicin released from antibiotic-loaded bone cement that ranges up to 50−100 $mg/\mu m^2$ within the first 10 min.[37] This implies that the high concentration of gentamicin released from the 3D-nanopillared surface only occurs at a very local region at the interface between the bacterium and the surface. The overall prevention of growth of *S. aureus* adhering on TA/G-coated 3D-nanopillared TiO_2 surfaces is effective, because gentamicin is released only in the low pH environment in the vicinity of an adhering staphylococcus.

Moreover, atomic force microscopy (AFM) measurement of bacterial adhesion force suggests that *S. aureus* should stay in a planktonic regime especially when sitting on the conical sharp tips of the bundled nanopillars. Figure 5 shows the bacterial adhesion forces measured with uncoated surfaces with different topographies. Staphylococci have the weakest adhesion (2 nN)

DOI: 10.1021/acsami.5b05947
ACS Appl. Mater. Interfaces 2015, 7, 20304−20313

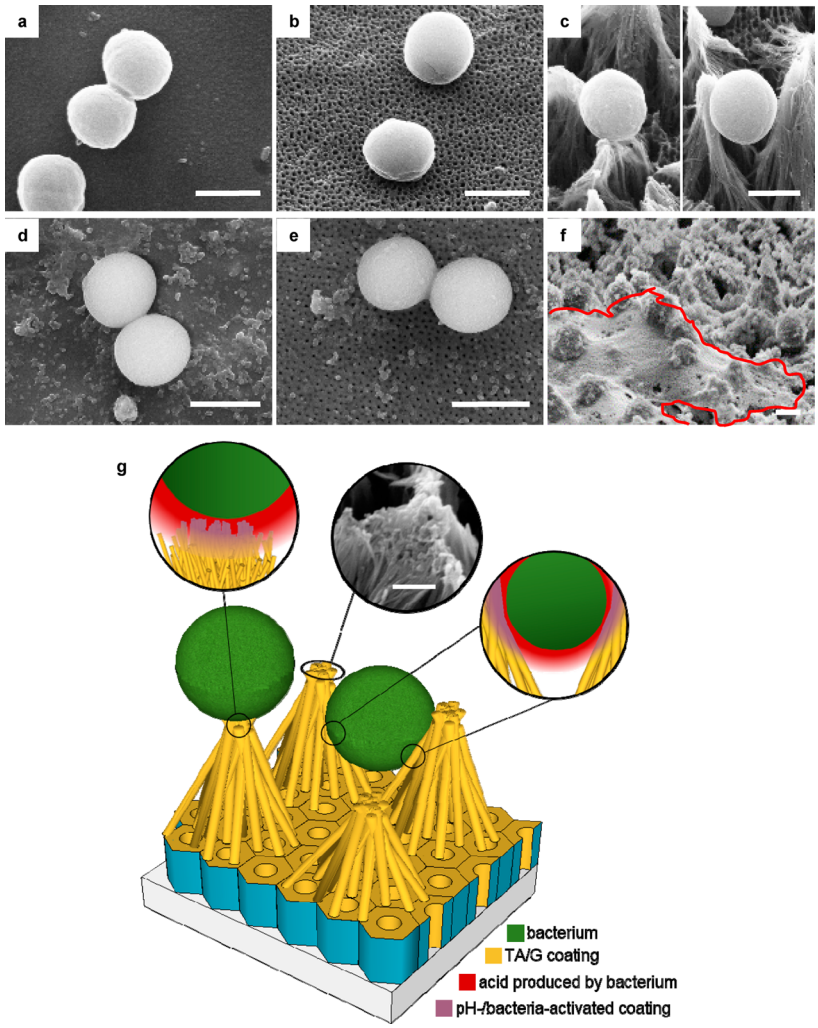

Figure 4. Appearance of bacteria adhering on nanostructured TiO_2 surfaces and proposed mechanism of antibiotic enhancement on 3D-nanostructured titanium. SEM images show *S. aureus* ATCC 12600 adhering to (a, d) smooth, (b, e) 2D-nanoporous, and (c, f) 3D-nanopillared TiO_2 surfaces in absence (top row) or presence (bottom row) of a gentamicin-coating (TA/G). Image c shows two different cases for bacterial adhesion: some bacteria tend to adhere on the nanopillar tips, whereas others reside in crevices. Note the appearance of patches of excreted extracellular polymeric substance (marked with a dashed line) on the TA/G-coated 3D-nanopillared surface (f). Scale bar in each SEM image indicates 1 μm. (g) Schematic of bacterial adhesion on the TA/G-coated 3D-nanopillared surface. The magnified scheme (top-left inset) depicts more detail of the nanopillars bundled at the top, as shown in the next inset of a SEM image (scale bar equals 50 nm).

on the 3D-nanopillared surface, compared to the smooth (8 nN) and 2D-nanoporous surfaces (4 nN). Meanwhile, the AFM measurement of coated surfaces was not practical because the gentamicin-containing coating killed the bacteria which were immobilized on the AFM cantilever tip when it approached to the coated surface. Although the absolute values of the adhesion force on coated surfaces would be different because of the different surface chemistry, the conclusion of the lower adhesion force on the 3D-nanopillared surface relative to the other surfaces should still be valid. Bacteria with low adhesion force are more prone to stay in planktonic regime and hence would leave the adhering staphylococci more susceptible to the antibiotics released.[38] In addition, the *S. aureus* adhering on the pointed tips of the 3D-nanopillared structures are prone to have more concentrated stress at the sharp contact. Such a sharp pointed contact would cause high membrane stress to the bacterium,[26] which also enhances antibiotic susceptibility and facilitates more efficient introduction of gentamicin into the bacterium.[38]

CONCLUSION

The anodizing process modulated with the hydrodynamic stirring speed and anodizing duration employed in this study allowed us to design and easily fabricate a hierarchical 3D-nanopillared surface on titanium which is superior to conventional 2D smooth or nanoporous surfaces. By depositing a "smart" bacteria-triggered self-defensive coating via the LbL technique on the 3D-nanostructures, a greater exposure of the antibiotic coating to adhering bacteria was provided and led to an increase in antibacterial efficiency of the LbL coating up to 10-fold compared to its performance on a smooth surface. Such a boost to the coating efficiency, enabled by 3D nanostructures, consequently allows a dramatic reduction in number of cycles used in coating deposition for the same efficacy. Furthermore, an additional advantage comes from the reduction of bacterial adhesion and an increase in their susceptibility to antibiotics when bacteria land on the 3D-nanopillared structures. The demonstrated strategy of a synergistic combination of advanced

DOI: 10.1021/acsami.5b05947
ACS Appl. Mater. Interfaces 2015, 7, 20304−20313

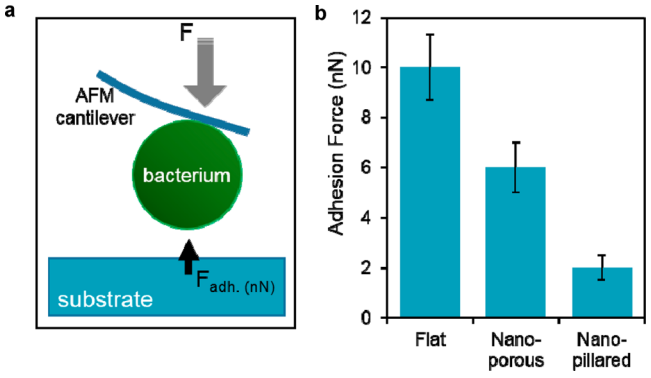

Figure 5. Atomic force microscopy (AFM) measurement of bacterial adhesion forces. (a) Scheme of bacterial-probe AFM with an immobilized bacterium attached on a tipless cantilever applied to measure staphylococcal adhesion forces. (b) Staphylococcal adhesion forces on smooth, 2D nanoporous and 3D nanopillared TiO_2 surfaces. Five measurements were taken on random locations on each substratum using a single *S. aureus* probe under an applied normal force of 5 nN in PBS buffer at pH 7.5.

3D nanostructuring and antibiotic coating holds great promise for engineering of bacteria-resistant biomedical implants.

METHODS AND MATERIALS

TiO_2 Nanostructure Fabrication. Titanium foils (4 cm × 1 cm, 0.5 mm in thickness, 99.6% purity, Alfa Aesar, Ward Hill, MA, USA) were degreased in metal cleaner solution (MC-3, Branson, Danbury, CT, USA), acetone and ethanol using an ultrasonic cleaner for 10 min and subsequently rinsed in deionized water and dried off with N_2 gas. Titanium foils were then electropolished in a solution of acetic acid (99.5%), sulfuric acid (98%) and hydrofluoric acid (40%) (60:15:25 in volume) at 1.40 A cm^{-2} at 20 °C for 1 min, followed by a chemical polishing in a mixture of HF (40%) and nitric acid (65%) (1:3 in volume) for 10 s to remove surface irregularities.

To create a 2D-nanoporous surface, we placed the electropolished TiO_2 foils in an insulated bath at 20 °C and anodized (see Figure 1) in an ethylene glycol solution containing NH_4F (0.38 wt %) and H_2O (1.79 wt %) for 15 min at 30 V using a DC power supply (Genesys 300−17, TDK-Lambda). The titanium foils were used as working electrodes (anode), and a platinum electrode was employed as a counter electrode (cathode). The two electrodes were separated at a distance of 5 cm. During the electrochemical process, the solution was stirred at 150 rpm unless stated otherwise using a magnetic stirrer to help maintain constant temperature and uniform anodization over the sample surface. After the anodizing step, each specimen was kept in absolute ethanol for 10 min and carefully rinsed in deionized water to remove the residue of the electrolytic solution.

For the preparation of a 3D-nanopillared surface (see also Figure 1), titanium foils were anodized for longer period (up to 4 h) at a much higher stirring speed of 2000 rpm.

The specimens were then imaged with a scanning electron microscope (FEI-SEM Quanta FEG450) to examine the surface topographies and uniformity of the nanostructures over the sample area (4 cm × 1 cm). The fabricated TiO_2 samples were diced into four pieces (1 cm × 1 cm for each) to allow multiple experiments for statistical analysis.

Deposition of a Gentamicin-Releasing Coating. The LbL technique for the preparation of the gentamicin-containing coating included sequential adsorption of tannic acid (TA) and gentamicin (G) from their solutions at pH 7.5 (see also Figure 1). Specifically, LbL films were deposited using a dipping robot (DR-3, Riegler & Kirstein GmbH, Berlin) operated with custom software. Smooth and/or nanostructured TiO_2 substrates were alternately immersed into 0.5 mg/mL of TA and 0.1 mg/mL of gentamicin solutions at pH 7.5 for 10 min, using three intermediate rinsing steps with 0.01 M phosphate buffer. All films contained gentamicin as the outermost layer. The growth mechanism of TA/G films has been described in detail elsewhere.[18] All coatings reported here were composed of 9 TA/G bilayers.

Bacterial Culture Conditions. From a frozen stock of *S. aureus* ATCC 12600 stored in 7% DMSO at −80 °C, bacteria were inoculated on blood agar plates and maintained for a maximum period of 12 days. Single colonies from the agar plates were inoculated in 10 mL tryptone soya broth (TSB, OXOID, Basingstoke, UK) and cultured for 18 h. This preculture was then used to inoculate a 200 mL main culture in TSB, which was grown for 16 h before harvesting. Bacteria were centrifuged twice at 5000 × g for 5 min at 10 °C, and washed with PBS (10 mM potassium phosphate, 0.15 M NaCl, pH 7.0) in between. *S. aureus* ATCC 12600 aggregates were separated by sonication on ice, three times for 10 s at 30 W (Vibra Cell model 375, Sonics and Materials Inc., Danbury, Connecticut, USA). Finally, staphylococci were suspended in 200 mL PBS to a density of 3×10^8 bacteria per ml as determined using a Bürker-Türk counting chamber.

Gentamicin Release. TA/G-coated TiO_2 samples were immersed in 0.5 mL pH 5.0 and pH 7.5 PBS, respectively, and incubated on a rotating table at 60 rpm up to 2 h at room temperature. After 10, 30, 60, and 120 min of incubation, respectively, 5 μL aliquots of the suspension were taken, and the antibiotic concentrations were determined by measuring the area of the inhibition zones around bacterially inoculated agar plates. Specifically, TSB agar plates were inoculated with a *S. aureus* ATCC 12600 suspension using a cotton swab. Ten minutes after inoculation, 5 μL of PBS or suspension aliquots were transferred to the center of each plate, and the plate was subsequently incubated aerobically at 37 °C. After 48 h incubation, clear areas around the position of the sample droplet indicated the absence of bacterial growth (see Figure S1). The diameters of these inhibition zones were measured in three perpendicular directions to calculate their areas and the amounts of gentamicin released per unit sample area using a calibration curve. To establish the calibration curve, we dissolved a known amount of gentamicin into five different PBS solutions and the corresponding gentamicin concentrations were calculated. Out of these gentamicin-containing PBS solutions, droplets (5 μL each) with the known antibiotic concentrations were put on agar plates which had initially been inoculated with *S. aureus* 12600. After 48 h incubation, the calculated antibiotic concentrations were related to the area of inhibition zones, which were developed because of the gentamicin-containing PBS droplets.

Bacterial Adhesion in a Parallel Plate Flow Chamber. Bacterial adhesion on the different TiO_2 surfaces was carried out in a parallel plate flow chamber (7.6 × 3.8 × 0.058 cm). The top glass and bottom PMMA plates of the chamber were placed in the middle of a stainless steel frame and separated by two Delrin spacers creating a smooth channel with a gradually diverging and converging (62 degrees) inlet and outlet region (see Figure S2). The chamber plates were sonicated for 3 min in 2% RBS35 (Omnilabo International BV, Breda, The Netherlands) followed by rinsing with tap water, demineralized water, methanol, tap water, and finally demineralized water. Prior to use, the flow chamber was washed with 2% Extran (Merck, Germany) and rinsed thoroughly with tap water and demineralized water.

Inserts were made in the bottom PMMA plate of the flow chamber, to allow placement of three different TiO_2 surfaces in a direction perpendicular to the flow. Note that coated and uncoated samples were never evaluated in one experiment. The locations of the smooth, 2D-nanoporous, and 3D-nanopillared surfaces were interchanged at each of triplicated adhesion experiments to compensate for possible differences in conditions at different locations on the bottom plate. Before each experiment, the flow chamber and tubes were first filled with PBS and all air bubbles were removed from the system. Next, the *S. aureus* ATCC 12600 suspension in PBS buffer was perfused through the flow chamber for 2 h under hydrostatic pressure at a laminar flow rate of 1 mL/min corresponding with a shear rate of 6 s^{-1}, whereas recirculating the suspension using a circulation pump. After 2 h, flow was switched to buffer at the same flow rate to remove nonadhering staphylococci from the system.

DOI: 10.1021/acsami.5b05947
ACS Appl. Mater. Interfaces 2015, 7, 20304−20313

Enumeration of Live and Dead Staphylococci. For enumeration, the adhering staphylococci were stained in the flow chamber with live/dead stain (*Bac*Light, Invitrogen, Breda, The Netherlands) for 15 min in the dark. The stock staining solution was prepared in a mixture of 3.34 mM SYTO 9 nucleic acid stain and 20 mM propidium iodide (1:1 in volume) for Live/Dead (Green/Red) viability. The stock solution was then diluted (24 μL to 8 mL of PBS) for staining. Five fluorescent images at different spots were taken from each triplicated samples using fluorescence microscopy (Leica DM4000B, Leica Microsystems GmbH, Heidelberg, Germany). Finally, the total number of adhering live and dead bacteria were counted using ImageJ software.

Statistical Analysis. The total numbers of adhering staphylococci and the numbers of viable organisms on the different surfaces were compared using a two-tailed Student's t test. Differences were considered significant if $p < 0.05$.

SEM Imaging of Staphylococcal Adhesion. Prior to electron microscope imaging of adhering staphylococci, TiO_2 surfaces were rinsed with PBS and then moved into a six-well plate. 2% glutaraldehyde was added and the plate was kept in a refrigerator at 4 °C overnight for fixation. Afterward, the surfaces were washed with 0.1 M cacodylate buffer, followed by 1 h of incubation at room temperature with 1% OsO_4 in 0.1 M cacodylate buffer. Subsequently, the samples were washed with deionized water and dehydrated with 30, 50, 70% ethanol for 15 min each and three times with absolute ethanol for 30 min at 4 °C. Finally, the samples were incubated in ethanol (100%) and tetramethylsilane (1:1) for 10 min, followed by 15 min incubation in pure tetramethylsilane and air-drying.

Bacterial Adhesion Forces. Bacterial adhesion forces on uncoated TiO_2 samples were recorded by using AFM (BioScope Catalyst atomic force microscope with ScanAsyst [Veeco Instruments Inc., Camarillo, CA]). Before each measurement, tipless cantilevers (NP-O10, Bruker AFM Probes, Camarillo, CA) were calibrated by the thermal tuning method, yielding an overall average spring constant of 0.047 ± 0.004 N m^{-1}. Bacterial probes were prepared by immobilizing single bacteria on a cantilever by using electrostatic attraction.[39] All adhesion force measurements were performed in PBS at room temperature with z-scan rates of 1.0 Hz under a loading force of 5 nN at 0 s surface delay. At least 10 force curves at the maximal adhesion force upon retraction were recorded at five randomly chosen spots and analyzed. To confirm that the bacterial probe was not damaged and not recording multiple contact values, we measured a force curve with 0 s surface delay on a bare glass that was then compared to control force curves that were recorded on glass initially. For each of the triplicated measurements, a new bacterial suspension was cultured and new bacterial probe was prepared.

■ ASSOCIATED CONTENT

Supporting Information

The Supporting Information is available free of charge on the ACS Publications website at DOI: 10.1021/acsami.5b05947.

Development of inhibition zones caused by gentamicin-containing droplets and schematic of a parallel plate flow chamber (PDF)

■ AUTHOR INFORMATION

Corresponding Author

*E-mail: cchoi@stevens.edu. Phone: 201-216-5579. Fax: 201-216-8315.

Present Address

[#]S.S. is currently at Department of Materials Science and Engineering, Texas A&M University, College Station, TX 77843, USA

Author Contributions

The manuscript was written through contributions of all authors. All authors have given approval to the final version of the manuscript. F.H. and C.-H.C. designed and fabricated the nanostructured samples. I.Z. and S.S. designed and deposited the antimicrobial coating. F.H., H.J.B., and H.C.M. designed and carried out the microbiology experiments. All authors contributed to analyzing the data.

Funding

This research was funded by Stevens Institute of Technology, Hoboken, NJ, and the University Medical Center Groningen, Groningen, The Netherlands.

Notes

The authors declare no competing financial interest.

■ ACKNOWLEDGMENTS

Authors thank the University of Medical Center, Groningen, The Netherlands for funding the double-PhD-degree position of FH. HJB is also director of a consulting company, SASA BV (GN Schutterlaan 4, 9797 PC Thesinge, The Netherlands). Opinions and assertions contained herein are those of the authors and are not construed as necessarily representing views of the funding organization or their respective employers.

■ REFERENCES

(1) Busscher, H. J.; van der Mei, H. C.; Subbiahdoss, G.; Jutte, P. C.; van den Dungen, J. J. A. M.; Zaat, S. A. J.; Schultz, M. J.; Grainger, D. W. Biomaterial-Associated Infection: Locating the Finish Line in the Race for the Surface. *Sci. Transl. Med.* **2012**, *4*, 153rv10−rv153rv10.

(2) Arciola, C. R.; Campoccia, D.; Speziale, P.; Montanaro, L.; Costerton, J. W. Biofilm Formation in Staphylococcus Implant Infections. A Review of Molecular Mechanisms and Implications for Biofilm-Resistant Materials. *Biomaterials* **2012**, *33*, 5967−5982.

(3) Costerton, J. W.; Lewandowski, Z.; Caldwell, D. E.; Korber, D. R.; Lappin-Scott, H. M. Microbial Biofilms. *Annu. Rev. Microbiol.* **1995**, *49*, 711−745.

(4) Ceri, H.; Olson, M. E.; Stremick, C.; Read, R. R.; Morck, D.; Buret, A. The Calgary Biofilm Device: New Technology for Rapid Determination of Antibiotic Susceptibilities of Bacterial Biofilms. *J. Clin. Microbiol.* **1999**, *37*, 1771−1776.

(5) Thitiyanaporn, C.; Thengchaisri, N.; Udomkusonsri, P. Comparison of Polymethylmethacrylate (PMMA), Native Calcium Sulfate, and High Porous Calcium Sulfate Beads as Gentamicin Carriers and Osteoblast Attachment. *Songklanakarin J. Sci. Technol.* **2013**, *35*, 293−301.

(6) Ismail, A. F.; Abdalmonemdoolaanea; Awang, M.; Mohamed, F. High Initial Burst Release of Gentamicin Formulated as PLGA Microspheres Implant for Treating Orthopaedic Infection. *Int. J. Pharm. Pharm. Sci.* **2012**, *4*, 685−691.

(7) Lowy, F. D. Antimicrobial Resistance: The Example of Staphylococcus Aureus. *J. Clin. Invest.* **2003**, *111*, 1265−1273.

(8) Pavlukhina, S.; Sukhishvili, S. In *Encyclopedia of Polymer Science and Technology*; John Wiley & Sons: New York, 2002.

(9) Nguyen, P. M.; Zacharia, N. S.; Verploegen, E.; Hammond, P. T. Extended Release Antibacterial Layer-by-Layer Films Incorporating Linear-Dendritic Block Copolymer Micelles. *Chem. Mater.* **2007**, *19*, 5524−5530.

(10) Chuang, H. F.; Smith, R. C.; Hammond, P. T. Polyelectrolyte Multilayers for Tunable Release of Antibiotics. *Biomacromolecules* **2008**, *9*, 1660−1668.

(11) Lichter, J. A.; Van Vliet, K. J.; Rubner, M. F. Design of Antibacterial Surfaces and Interfaces: Polyelectrolyte Multilayers as a Multifunctional Platform. *Macromolecules* **2009**, *42*, 8573−8586.

(12) Moskowitz, J. S.; Blaisse, M. R.; Samuel, R. E.; Hsu, H.-P.; Harris, M. B.; Martin, S. D.; Lee, J. C.; Spector, M.; Hammond, P. T. The Effectiveness of the Controlled Release of Gentamicin from Polyelectrolyte Multilayers in the Treatment of Staphylococcus Aureus Infection in a Rabbit Bone Model. *Biomaterials* **2010**, *31*, 6019−6030.

DOI: 10.1021/acsami.5b05947
ACS Appl. Mater. Interfaces 2015, 7, 20304−20313

(13) Wong, S. Y.; Moskowitz, J. S.; Veselinovic, J.; Rosario, R. a; Timachova, K.; Blaisse, M. R.; Fuller, R. C.; Klibanov, A. M.; Hammond, P. T. Dual Functional Polyelectrolyte Multilayer Coatings for Implants: Permanent Microbicidal Base with Controlled Release of Therapeutic Agents. *J. Am. Chem. Soc.* **2010**, *132*, 17840−17848.
(14) Lv, H.; Chen, Z.; Yang, X.; Cen, L.; Zhang, X.; Gao, P. Layer-by-Layer Self-Assembly of Minocycline-Loaded Chitosan/Alginate Multilayer on Titanium Substrates to Inhibit Biofilm Formation. *J. Dent.* **2014**, *42*, 1464−1472.
(15) Schmaljohann, D. Thermo- and pH-Responsive Polymers in Drug Delivery. *Adv. Drug Delivery Rev.* **2006**, *58*, 1655−1670.
(16) Ganta, S.; Devalapally, H.; Shahiwala, A.; Amiji, M. A Review of Stimuli-Responsive Nanocarriers for Drug and Gene Delivery. *J. Controlled Release* **2008**, *126*, 187−204.
(17) Balamuralidhara, V.; Pramodkumar, T. M.; Srujana, N.; Venkatesh, M. P.; Vishal Gupta, N.; Krishna, K. L.; Gangadharappa, H. V. pH Sensitive Drug Delivery Systems: A Review. *Am. J. Drug Discovery Dev.* **2011**, *1*, 24−48.
(18) Zhuk, I.; Jariwala, F.; Attygalle, A. B.; Wu, Y.; Libera, M. R.; Sukhishvili, S. A. Self-Defensive Layer-by-Layer Films with Bacteria-Triggered Antibiotic Release. *ACS Nano* **2014**, *8*, 7733−7745.
(19) Wang, Y.; Subbiahdoss, G.; Swartjes, J.; van der Mei, H. C.; Busscher, H. J.; Libera, M. Length-Scale Mediated Differential Adhesion of Mammalian Cells and Microbes. *Adv. Funct. Mater.* **2011**, *21*, 3916−3923.
(20) Bos, R.; Van Der Mei, H. C.; Gold, J.; Busscher, H. J. Retention of Bacteria on a Substratum Surface with Micro-Patterned Hydrophobicity. *FEMS Microbiol. Lett.* **2000**, *189*, 311−315.
(21) Popat, K. C.; Eltgroth, M.; Latempa, T. J.; Grimes, C. A.; Desai, T. A. Decreased Staphylococcus Epidermis Adhesion and Increased Osteoblast Functionality on Antibiotic-Loaded Titania Nanotubes. *Biomaterials* **2007**, *28*, 4880−4888.
(22) Puckett, S. D.; Taylor, E.; Raimondo, T.; Webster, T. J. The Relationship Between the Nanostructure of Titanium Surfaces and Bacterial Attachment. *Biomaterials* **2010**, *31*, 706−713.
(23) Ercan, B.; Taylor, E.; Alpaslan, E.; Webster, T. J. Diameter of Titanium Nanotubes Influences Anti-Bacterial Efficacy. *Nanotechnology* **2011**, *22*, 295102.
(24) Wu, Y.; Zitelli, J. P.; TenHuisen, K. S.; Yu, X.; Libera, M. R. Differential Response of Staphylococci and Osteoblasts to Varying Titanium Surface Roughness. *Biomaterials* **2011**, *32*, 951−960.
(25) Tang, P.; Zhang, W.; Wang, Y.; Zhang, B.; Wang, H.; Lin, C.; Zhang, L. Effect of Superhydrophobic Surface of Titanium on Staphylococcus Aureus Adhesion. *J. Nanomater.* **2011**, *2011*, 1−8.
(26) Ivanova, E. P.; Hasan, J.; Webb, H. K.; Gervinskas, G.; Juodkazis, S.; Truong, V. K.; Wu, A. H. F.; Lamb, R. N.; Baulin, V. a; Watson, G. S.; Watson, J. a; Mainwaring, D. E.; Crawford, R. J. Bactericidal Activity of Black Silicon. *Nat. Commun.* **2013**, *4*, 2838.
(27) Hizal, F.; Rungraeng, N.; Jun, S.; Choi, C.-H. In *Proceedings of the 9th IEEE International Conference on Nano/Micro Engineered and Moleculer Systems*; Honolulu, HI, April 14−16, 2014 IEEE: Piscataway, NJ, 2014; pp 17−22.
(28) Pérez-Jorge, C.; Conde, A.; Arenas, M. a; Pérez-Tanoira, R.; Matykina, E.; de Damborenea, J. J.; Gómez-Barrena, E.; Esteban, J. In vitro Assessment of Staphylococcus Epidermidis and Staphylococcus Aureus Adhesion on TiO_2 Nanotubes on Ti-6Al-4V Alloy. *J. Biomed. Mater. Res., Part A* **2012**, *100*, 1696−1705.
(29) Yang, L.; Luo, S.; Cai, Q.; Yao, S. A Review on TiO_2 Nanotube Arrays: Fabrication, Properties, and Sensing Applications. *Chin. Sci. Bull.* **2010**, *55*, 331−338.
(30) Shin, H. G.; Park, Y. M.; Kim, B. H.; Seo, Y. H. Fabrication of Hemispherical Nano Structure on a Curved Al Surface Using Low-Temperature and High-Voltage Anodizing Method. *J. Nanosci. Nanotechnol.* **2011**, *11*, 427−431.
(31) Aimi, M. F.; Rao, M. P.; MacDonald, N. C.; Zuruzi, A. S.; Bothman, D. P. High-Aspect-Ratio Bulk Micromachining of Titanium. *Nat. Mater.* **2004**, *3*, 103−105.
(32) McEligoi, D. M. Fundamentals of Momentum, Heat and Mass Transfer. *Int. J. Heat Mass Transfer* **1970**, *13*, 1641−2213.
(33) Roy, P.; Berger, S.; Schmuki, P. TiO_2 Nanotubes: Synthesis and Applications. *Angew. Chem., Int. Ed.* **2011**, *50*, 2904−2939.
(34) Lim, J. H.; Choi, J. Titanium Oxide Nanowires Originating from Anodically Grown Nanotubes: The Bamboo-Splitting Model. *Small* **2007**, *3*, 1504−1507.
(35) Jeong, C.; Choi, C.-H. Single-Step Direct Fabrication of Pillar-on-Pore Hybrid Nanostructures in Anodizing Aluminum for Superior Superhydrophobic Efficiency. *ACS Appl. Mater. Interfaces* **2012**, *4*, 842−848.
(36) Chevalier, J.; Gremillard, L. Ceramics for Medical Applications: A Picture for the Next 20 Years. *J. Eur. Ceram. Soc.* **2009**, *29*, 1245−1255.
(37) Neut, D.; van de Belt, H.; van Horn, J. R.; van der Mei, H. C.; Busscher, H. J. The Effect of Mixing on Gentamicin Release from Polymethylmethacrylate Bone Cements. *Acta Orthop. Scand.* **2003**, *74*, 670−676.
(38) Muszanska, A. K.; Nejadnik, M. R.; Chen, Y.; van den Heuvel, E. R.; Busscher, H. J.; van der Mei, H. C.; Norde, W. Bacterial Adhesion Forces with Substratum Surfaces and the Susceptibility of Biofilms to Antibiotics. *Antimicrob. Agents Chemother.* **2012**, *56*, 4961−4964.
(39) Camesano, T. A.; Natan, M. J.; Logan, B. E. Observation of Changes in Bacterial Cell Morphology Using Tapping Mode Atomic Force Microscopy. *Langmuir* **2000**, *16*, 4563−4572.

DOI: 10.1021/acsami.5b05947
ACS Appl. Mater. Interfaces 2015, 7, 20304−20313